Desalination. Volume 486, March 2020, 114407. DOI:10.1016/j.desal.2020.114407

The polymeric conformational effect on capacitive deionization performance of graphene oxide/polypyrrole composite electrode

Ke Xu[a,]*, Yanhui Liu[a,] *, Zihan An[a], Ashok J. Gadgil [b, c], Guorong Xu[a] and Guoling Ruan[a]

Associate Prof. Ke Xu

[a]The Institute of Seawater Desalination & Multipurpose Utilization, MNR, Tianjin 300192, PR China

e-mail address: xukeler@hotmail.com.

*corresponding author

Dr. Yanhui Liu

[a]The Institute of Seawater Desalination & Multipurpose Utilization, MNR, Tianjin 300192, PR China

e-mail address: hildaliuliu@163.com.

*This author contributed equally to this work

Dr. Zihan An

[a]The Institute of Seawater Desalination & Multipurpose Utilization, MNR, Tianjin 300192, PR China

e-mail address: tjdhsazh@163.com.

Prof. Ashok J. Gadgil

[b]Energy Technologies Area, Lawrence Berkeley National Laboratory and

[c]Civil and Environmental Engineering, University of California, Berkeley,

Berkeley CA 94720

e-mail: ajgadgil@lbl.gov

Associate Prof. Guorong Xu

[a]The Institute of Seawater Desalination & Multipurpose Utilization, MNR, Tianjin

300192, PR China
e-mail address: labxgr@sina.com.

Prof. Guolin Ruan

[a]The Institute of Seawater Desalination & Multipurpose Utilization, MNR, Tianjin

300192, PR China
e-mail address: glruan@263.net.

Abstract

Exploitation of novel faradic electrode materials is an alternative implementation for solving the problem of poor specific electrosorption capacity that conventional carbon-based electrodes are encountered in capacitive deionization. Particularly, composite electrode is just an suitable choice because of its potentially high ion-storage ability. Herein, a cyclic voltammetric treatment method with different low limit of potential window were used to manipulate the polymeric conformation and doping level of graphene oxide/polypyrrole (GO/PPy) composite electrode. Based on it, the effect of polymeric structure on the electro-sorption performance was systematically studied. When the low limit of potential window is shifted to a potential negative enough, the irreversible polymeric conformational shrinks of GO/PPy electrode are promoted, which not only hinders the insertion process of ions

in the composite matrix, but also decrease the doping level of polymer due to the intensive interchain interaction produced by more entangled polymeric chain. Thus, the number of intercalated ions should decrease, which is expressed by EIS results and is proportional to the electro-sorption capacity of GO/PPy composite electrode in MCDI process. Our work suggest that the less packing density, higher doping level and more charge delocalization on PPy backbone in composite electrode is beneficial to enhance its capacitive deionization performance.

1. Introduction

Population growth, effects of climate change, and improved standards of living all contribute to the growing global energy and freshwater shortages. Various desalination technologies have been successful developed for desalting seawater, but they are all energy intensive [1,2]. One approach to reducing energy demands of desalination is through the effective treatment of non-sea saline sources known as "brackish water" [3]. In this context, capacitive deionization (CDI) has been shown to be both lower-cost and lower-energy compared with the widely-used reverse osmosis (RO) technology for brackish water (TDS≤3g/L) desalination [4,5]. CDI technology relies on the charge storage in the electric double layer (EDL) developed when salt ions are attracted onto porous electrodes using an external D.C. voltage, the ions are subsequently desorbed (into a reject concentrated brine) by reversing the polarity of the external voltage or short-circuiting the cell [6]. The promise of high energy efficiency, low electrode fouling, easy operation, attracts more interesting in the application of brackish water desalination and industrial wastewater treatment.

Despite the advantages presented by CDI relative to other commercial technologies, there are still several aspects of it that require research and development before its widespread commercial application, especially the electrode materials. A good

candidate for it to be used must have high adsorption capacity, high electron or ion transfer rate and low cost [6,7]. In this respect, the graphene-conducting polymer composite, which have triggered considerable interest in the field of supercapacitor and energy storage, should be suitable for CDI electrode due to the ultrahigh areal capacitance benefited from the synergistic effect of the good conductive graphene backbone and high pseudocapacitive conducting polymer [8]. For example, a three-dimensional graphene foam fabricated by chemical vapor deposition on nickel foam as the growth substrate, is a good support for deposition of large quantities of polyaniline (PANI). The high porosity of hybrid network renders a large areal capacitance of about 1.7 $F \cdot cm^{-2}$, it is more than double that of the pure graphene foam or PANI thin layer [9]. Xin et al. used the in-site grown graphene by electrochemical exfoliation of flexible graphite sheet as an alternative support to prepare hybrid network, which exhibited a maximum areal capacitance of 1.36$F \cdot cm^{-2}$[10]. Three-dimensional stacking of PANI porous layer anchored pillared graphene sheet [11], or PANI-PSS nanoparticles intercalated graphene sheet [12], also exhibites similar capacitive responses, because steric hindrance of the conducting polymer helps the graphene sheets to stay apart. As for GO/PPy composite material, it may has high charge-discharge capacity in principle due to the nature of peudocapacitance characteristics. In the past, we have fabricated the GO/PPy composite electrode by one-step coelectrodepostion in GO/pyrrole micelle, in which the benzenesulfonic sodium (BS) was added and acted as secondary dopant for improving the electrochemical activity of hybrid materials [13]. From the cyclic-voltammetry, the areal capacitance was 1.286 $F \cdot cm^{-2}$ at the mass density of 8.3mg/cm^2, which is close to the graphene/PANI composites.

Furthermore, in principle, the graphene/PPy composite may be more suitable for CDI application than graphene/PANI, because the proton acid doping nature of PANI shall induce the electrochemical activity deterioration in neutral salt solution [14,15]. Instead,

the doping/dedoping of PPy is based on the electron-transfer mechanism in the electrochemical redox and the concomitant counter-ion migration to neutralize residual charge on polymer chain, which is low dependent of solution pH [16]. The coating-type carbon nanotube/PPy electrode by compression molding of the composite power exhibited the high specific adsorption capacity of 72.36mg/g [17], which was superior to that of active carbon/PANI [18]. Even though in strong acid or alkaline solution, PPy has also shown good electrochemical redox stability[19].. However, the structural effect of conducting polymer component can exert more obvious influence on the adsorption capacity of composite than solution pH. For example, once the dodecylbenzene sulfonate dopant of PPy was replaced with Cl^-, the specific adsorption of composite declined to only 40.8mg/g [17]. But up to now, there is few in-depth research on this structural effect, which is extremely adverse to the sustained development of graphene/conducting polymer for CDI application. In this work, cyclic voltammetric treatment method with different low limit of potential window[20] were used to manipulate the polymeric conformation and doping level of PPy in composite electrode. And the morphologies, chemical structure, electrochemical characteristic as well as CDI performance of GO/PPy with and without deep reduction (named as DR-GO/PPy and non-DR-GO/PPy) were examined. By analyzing the corresponding relationships between polymeric conformational and the electro-sorption performace of composite electrode, it will be useful to better understand the electro-sorption process of faradic GO/PPy composite materials, such as electron transfer between the current collector and PPy to form charge delocalization(e.g., polarons and bipolarons) and ions transfer from the solution or from the film to maintain charge neutrality in the composite matrix, and is helpful to improve this novel faradic CDI electrode performance from polymeric structual sense.

2. Experimental

2.1 Electrodepositon of GO/PPy on carbon fiber paper

The freshly distilled pyrrole (335mg) was added into 50mL GO colloid solution with concentration of 0.3mg/mL, and rapid stirred for 4h to form GO/pyrrole solution. After that, the different amount of benzenesulfonate sodium was added and stirred for 1h to control the size distribution of GO/pyrrole micelles. Finally, the pH value of the solution was adjusted to 3 by using benzenesulfonic acid. Electrochemical polymerizations were performed by a galvanostatic method in three-electrode cell equipped with a carbon fiber papers as the working electrode (apparent surface area of 25cm^2), a platinum sheet as the counter electrode and a standard calomel electrode (SCE) as the reference electrode. The deposition current density of 2mA/cm2 and the polymerization charge of 10C/cm^2 was selected. After that, the electrode was ultrasonic washed thoroughly with deionized water, and dried under vacuum at 60 °C before used. All the solutions were degassed with nitrogen gas for 30 min before used, and a nitrogen atmosphere was kept during the preparation of GO/pyrrole micelle solution, electropolymerization and electro-reduction processes.

2.2 Manipulation of polymer chain structure by electrochemical techniques

The as-prepared GO/PPy electrode was electrochemical washed by cyclic voltammetric method with the potential window of 0 to -0.4 V (vs. SCE) in 1.0 M KCl at scan rate of 5 mV/s. And the benzenesulfonate dopants in composite film were gradually substituted by chloride ions, which composite was named as non-DR-GO/PPy.. The DR-GO/PPy electrode was performed by negative shifted the low limit of potential window from -0.4V to -1.0 V (vs. SCE) in 1.0 M KCl at scan rate of 5 mV/ s. And the cyclic scan repeated least five times till the subsequent cyclic voltammetric curves almost overlapping. All of the electrochemical operation were conducted on Biologic VMP3 electrochemistry station.

2.3 Structure and morphology characterization

Fourier transform infrared spectra (FT-IR) of different GO/PPy specimens were recorded on a Bruker Vector 22 spectrometer with in-situ measurement accessories. X-ray photoelectron spectra (XPS) were recorded on a Thermo K-Alpha photoelectron spectrometer, using Al Kα X-ray as the excitation source. The microstructural morphologies and elements of these specimens were analyzed on a Hitachi TM3030 desktop scanning electron microscope (SEM) at an accelerating voltage of 15kV and on an Bruker Quantax energy spectrum analyzer (EDS) at an accelerating voltage of 30kV, respectively.

2.4 The EIS measurements and specific capacitance calculation

The electrodes used in electrochemical impedance spectroscopy (EIS) measurements were cut off from above-mentioned specimens, and each surface area of the working electrodes was $2cm^2$. The counter electrode was a platinum sheet, and the reference electrode was a standard calomel electrode (SCE). The EIS were carried out at the dc potential range of -0.4 to 0.8V vs. SCE, the frequency range was from 100 kHz to 10 mHz with an sinusoidal voltage perturbation of 10mV. A steady electrochemical state of composite electrode before EIS analysis was obtained by waiting 15 min at each D.C. potential. The specific capacitance (C) were calculated from the imaginary part (Z') and angular frequency (ω) of the impedance data at the frequency of 0.01Hz by the Eq. (1) [21].

$$C = \left| \frac{1}{\omega Z''} \right| \qquad (1)$$

The specific capacitance was normalized by the minimum capacitance over the potential range, and the PZC is the potential at the minimum of the normalized capacity vs. potential plot where $C/C_{min} = 1$.

2.5 MCDI performance tests

To investigate the structural effect of PPy on the electrosorption performance of the composite electrodes, an experimental flow-through type membrane CDI (MCDI) cell was configured in the following order: end plastic plate/ current collector (graphite)/ positive electrode/ anion-exchange membrane/ separator/ cation-exchange membrane/ negative electrode/ current collector (graphite)/ end plastic plate (as shown in Fig.1). The NaCl aqueous solutions with concentration range of 200~1000 mg/L were used as the feed water of MCDI cell. And the volume of feed water in reservoir was more than 20L, which could decrease the influence of feed water concentration slight fluctuation result from the effluent returning to feed water reservoir. The inlet flow rate was set to 20mL/min by a peristaltic pump (Masterflex L/S, Cole–Parmer, USA). The electrical conductivity of effluent was monitored every 1s by an online conductivity sensor (Thornton UniCond 2-E, Mettler-Toledo, USA). The relationship between conductivity (μS/cm) and concentration (mg/L) was obtained from a pre-determined calibration curve prior to the experiment.

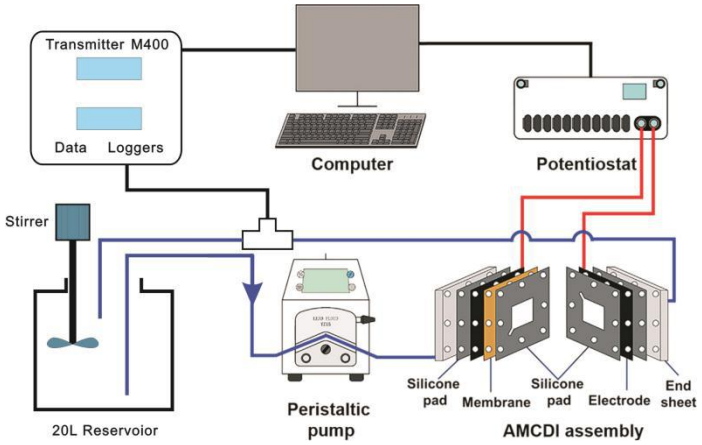

Fig.1. Flow diagram representation of the MCDI experimental setup composed of a deionization cell, sensors, and pump.

3. Results and discussion

3.1. Morphological analysis

SEM characterization was used to investigate the structure and morphology of non-DR-GO/PPy and DR-GO/PPy in Fig.2. As clearly seen from Fig.2a and 2b, the as-prepared GO/PPy and non-DR-GO/PPy has the obvious 3D cauliflower-fungus-shape structure, in which many GO nanosheet were bent and coiled to form a flocculent multiporous precipitate. These structural characteristics were similar as that of high surface area graphene fabricated by exothermic approach with metal Li and CO_2 at 550℃, and seemed to be beneficial to improve the areal capacity [22]. If the GO/PPy was deep reduced , the flocculent GO fragments were expelled from the composite driven by the electric field and the polymer conformational shrinkage. The lamellar GO nanosheets with large scale and compact texture had been retention in the composite matrix, as shown in Fig.2c. These morphology variation are somewhat similar as PPy conformational change after electrochemical oxidation degradation process [23], and can be reasonable speculated that it is associated with the volume shrink and pore dimension increase of the polymer component in composite electrode.

The component and element distributions were evaluated by EDS in Fig.S1 and S2, S3 (shown in Supporting information). The ultrasonic washing could not remove the benzenesulfonate ion in the composite matrix, and the S element homogeneous distributed in the composite electrode as shown in Fig.S1, however, it was not detected in the non-DR-GO/PPy and DR-GO/PPy. It means that the as-prepared GO/PPy composite have not been densely packed as previous reported PPy doped with aromatic sulfonate anions [24], in which aromatic sulfonate anions exhibited good mobility even the strong electrostatic and aromatic stacking interaction between PPy and benzenesulfonate ion. This characteristic made it possible to evaluate the effect of polymeric chain conformation on the electrosorption performance after electro-chemical treatment by cyclic voltammetry with different low limit of the potential window.

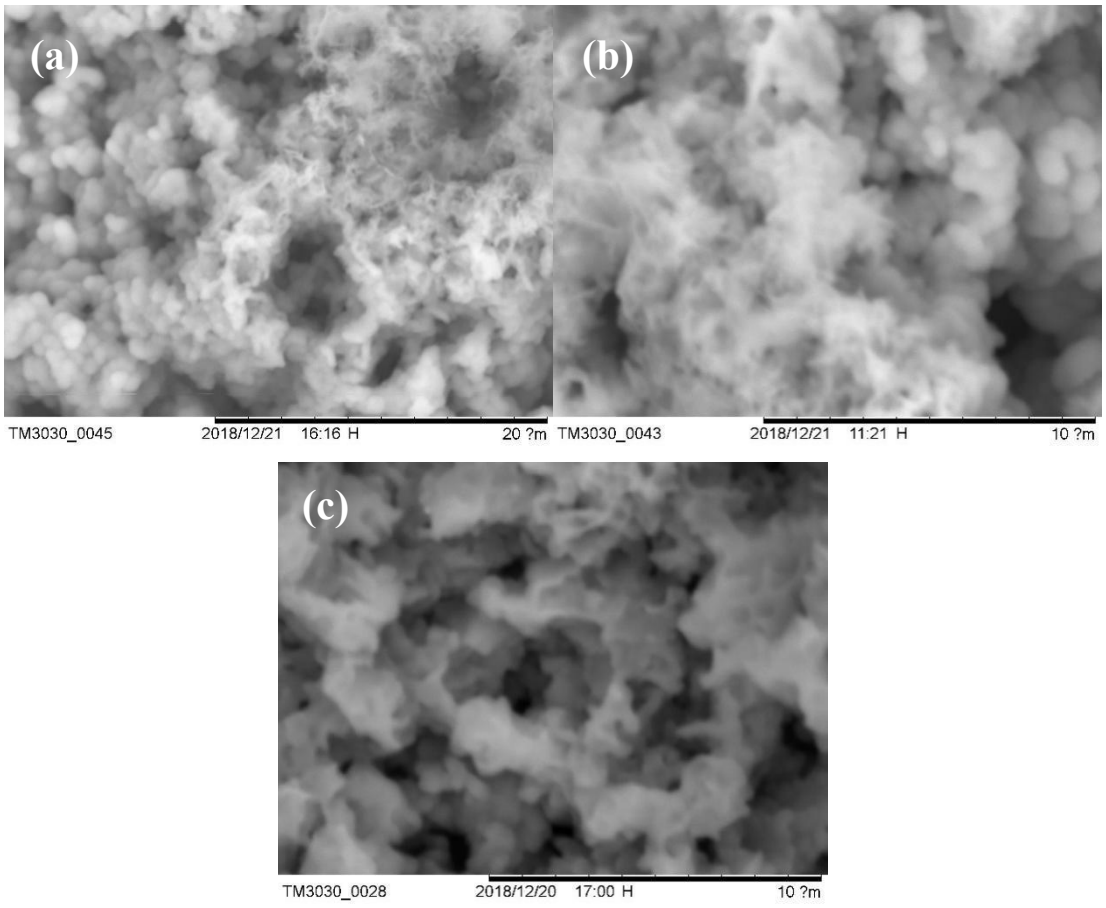

Fig.2. SEM images of as-prepared GO/PPy specimens after only ultrasonic washing(a), non-DR-GO/PPy (b), and DR-GO/PPy (c).

3.2 Chemical and structural analysis

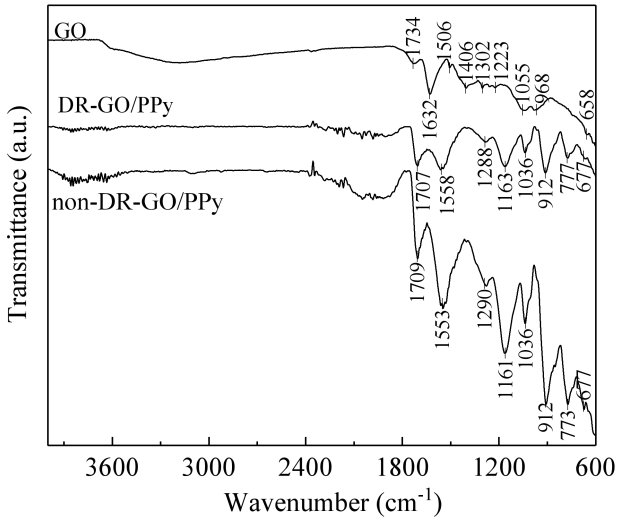

Fig. 3. FTIR spectrum of GO, non-DR-GO/PPy and DR-GO/PPy.

The FTIR spectra of the GO, non-DR-GO/PPy and DR-GO/PPy composite were presented in Fig. 3a. From the top spectrum, the IR peaks of pristine GO agree well

with the literature [25], including broad and intense peak at 1632cm^{-1} assigned to the C=C stretching vibration, peak at 1734cm^{-1} to C=O (carboxyl) stretching vibration, and peaks at 1406, 1223 and 1055cm^{-1} assigned to the O-H deformation, the carboxyl (C-OH) and epoxide (C-O-C) groups, respectively. In the case of non-DR-GO/PPy specimens, several new peaks attributed to PPy appeared in the spectrum as presented in literature [25, 26]. Characteristic peaks at 1553, 1290, 1036, 912, 773cm^{-1} are typical characteristic peaks of PPy with different vibration modes[26]. It should be note that the C=O group peak of non-DR-GO/PPy has downshifted to 1709cm^{-1}, which is probably due to the π-π interactions and hydrogen bonding between the GO nanosheets and heterocyclic PPy rings. It suggests that the carboxyl groups from GO acted as one kind of dopant and GO has been successfully wrapped with PPy film [27]. As for the DR-PPy/GO, the peak at 1709cm^{-1} was weakened and shifted to 1707cm^{-1}, and the peak at 1553cm^{-1}, antisymmetric ring (C-C) stretching vibration in the PPy, shifted to 1558cm^{-1}. The blue shift and weakening of C-C stretching peak of PPy ring in DR-GO/PPy composite may be related to the structural change in packed density and chemical environmental variation, and is considered to be indicative of decreasing degree of charge delocalization on the PPy backbone due to less doped level and/or increased inter-chain interactions.

The XPS is used to study this structural variation of GO/PPy matrix during the deep reduction process. Fig.4 shows the wide region and the C1S core level spectra of the GO, as-prepared GO/PPy, non-DR-GO/PPy and DR-GO/PPy. Due to the different chemical environments of carbon atoms in composite, the asymmetric C1s main peaks are fitted into four or five gaussian peaks. The high binding energy peaks of as-prepared GO/PPy at 290.5eV and 288.1eV are assigned to the O-C=O and C=O groups respectively, suggesting that the over-oxidation of GO and/or PPy component may have occurred during the electropolymerization [28]. The peak with lowest binding energy at 283.7eV is related to the carbon atoms bonded with sulfur on the

doped benzene ring [29]. And its disappearance after electrochemical washing by cyclic voltammetry shows that the sulfonate ion has been completely ejected from matrix, which is match with the wide region scanning XPS spectra shown in Fig.4e. While the two deconvoluted gaussian peaks at 284.6-284.7eV and 285.4-285.5eV originate from the pyrrole β carbon (C-C/C=C), graphene oxide carbon and α carbon (C-N) [29]. And the guassian peak at 286.5-286.6eV causes the asymmetric spectra on the higher binding energy side, and is attributed to a general disorder type of carbon.

The area percentage of disorder carbon peak is 12.5% for as-prepared GO/PPy, which is as much as the electrochemical synthesized partially exfoliated graphene/PPy (doped with 2-naphehalene sulfonate) composite electrode by Song [29]. Constantly, the “disorder effect” was attributed to interchain crosslinks, side chains, chains end, and carbon in partial unsaturated rings. If the oxidized polymerization process of PPy is not under the mild conditions, such as chemically synthesized PPy by APS and electrochemically synthesized PPy, the degree of disorder carbon will increase significantly [30]. When the low limit of potential window in cyclic voltammetric treatment is negative shifted, the area percentage of the disorder peak rises gradually (the percentage of non-DR-GO/PPy and DR-GO/PPy is 16.3% and 19.0%, respectively). Of course, these phenomenon observed for non-DR-GO/PPy and DR-GO/PPy is not due to the chemical bonding between neighboring polymeric chain, but to the increased inter-chain interaction, e.g. van der Waals force or hydrogen bonding, arising from the densely chain entanglement. Generally, beside the polymerization process, PPy interchain chemical crosslinking take place only at the degradation process once the application potential is above 0.58V (vs. SCE) [23]. The irreversible volume shrink of polymer matrix and transfer hindrance of ions insertion in overoxidation is somewhat similar as above-mentioned phenomenon, but the application potential condition is not agree with this work. On the other hand, the reduction process of PPy at negative potential is constantly accompanied by

conformation shrinking and counterions moving toward the solution by diffusion control. As the reduction process continues, the structure of the polymer is closed before the completed reduction. If much higher overpotential is applied, the polymeric chain rearrangement is promoted to continuous shrink volume and eject residual counterions under conformation kinetic control[20], which would decrease the polymeric interchain separation and strengthen the intermolecular force. This stronger interchain force can limit the chain entanglement structure opened and the charge delocalization along the polymer backbone at the subsequent oxidation process, and then is prone to decrease the doping levle and charging density of PPy. Correspondingly, the specific peak areas ratio of the XPS spectra is calculated for materials doping level characterization. As listed in Tab.1, the [S]/[N] percentage of as-prepared GO/PPy and the [Cl]/[N] percentage of non-DR-GO/PPy is 45.4% and 46.1%, respectively, while the [Cl]/[N] percentage of DR-GO/PPy decline to nearly half of the value. It can be concluded that the deep reduction process can induce the polymeric chain entanglement and strengthen the inter-molecular force, which leads to the increase of "disorder carbon" and decline of doping level.

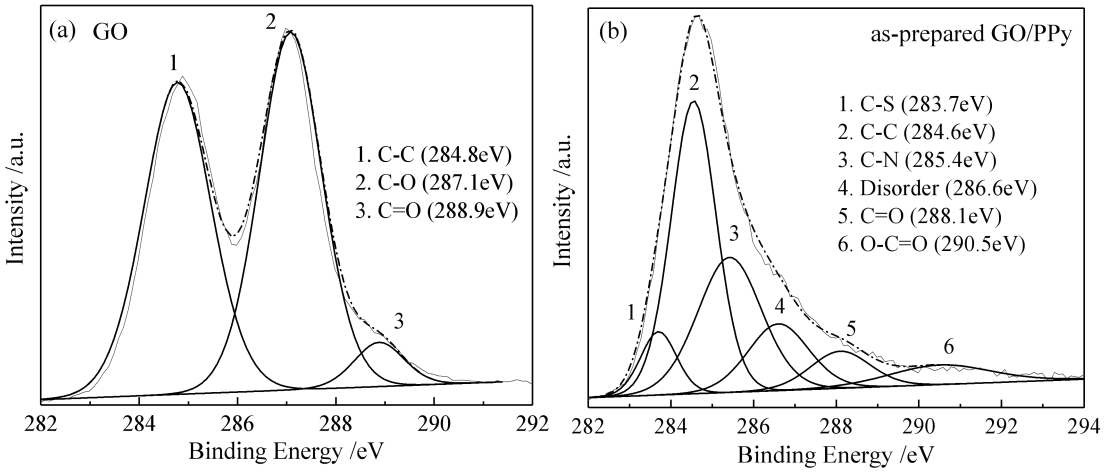

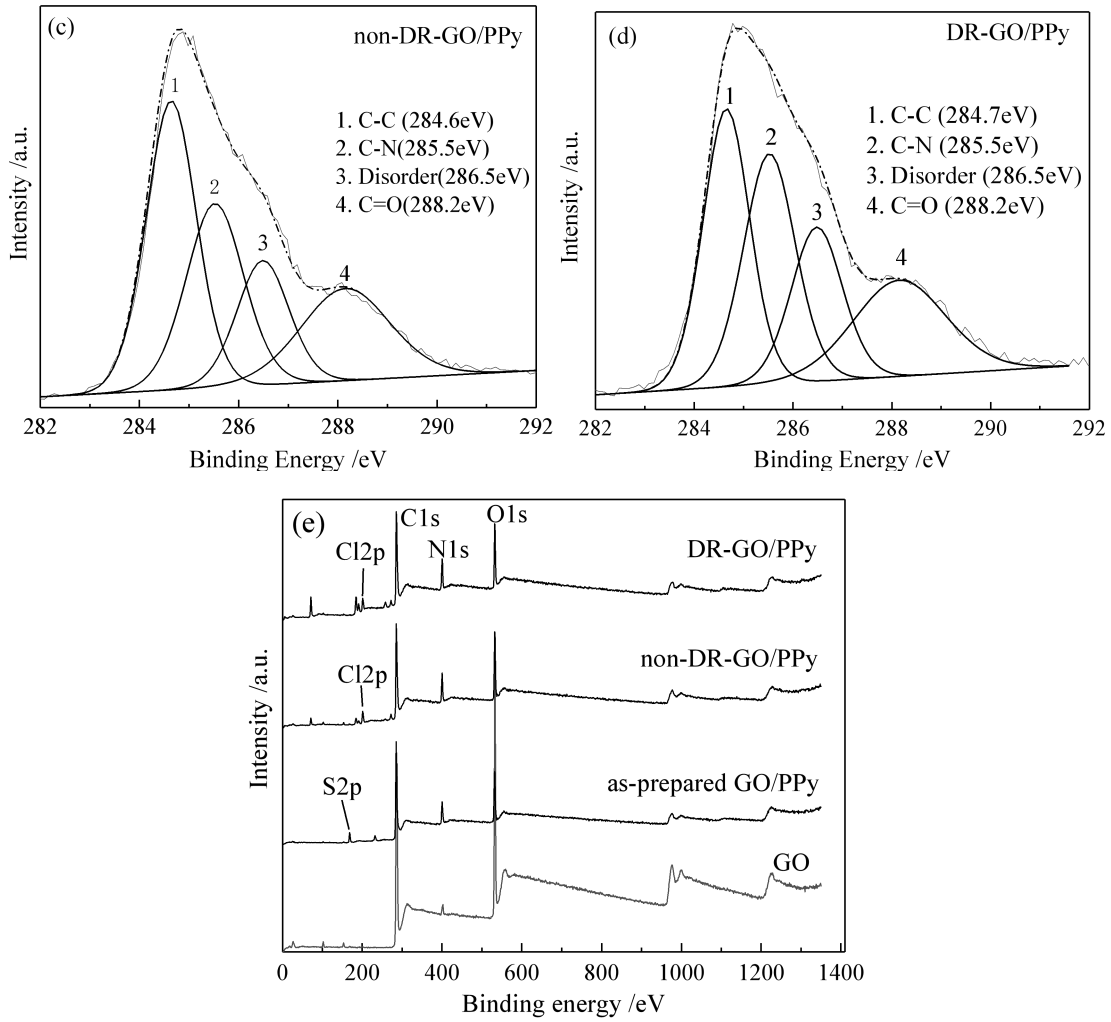

Fig. 4. The C1s XPS core level spectra (a-d) and wide region scanning XPS spectra (e) of GO, as-prepared GO/PPy, non-DR-GO/PPy and DR-GO/PPy electrode.

Tab.1. Atomic percentage of elements on the surface of the electrode materials

Sample	C(atom%)	N(atom%)	O(atom%)	S(atom%)	Cl(atom%)	S/N or Cl/N (atom%)
as-prepared GO/PPy	71.56	8.90	15.50	4.04	/	45.39
non-DR-GO/PPy	67.33	10.49	17.34	/	4.84	46.12
DR-GO/PPy	63.31	11.26	16.25	/	3.18	28.24

3.3 The EIS analysis for two electrodes

EIS is used to evaluate charge transfer process of the two GO/PPy composite electrodes. The Nyquist plots of the two electrodes at the d.c. potential range of -0.4~0.5V displayed in Fig.5a show the similar distorted semi-circle at the high-frequency region and nearly vertical linear line at the low frequency region, which is typical for capacitive materials. When the d.c. potential rises up to 0.6V and above, the degradation of PPy take place more or less and turns the low-frequency non-faradic impedance responses more complex[23]. The charge transfer resistance (R_{ct}), constantly used to reflect the electronic conductivity of composite and the ionic electro-sorption kinetics at the outer layer of the electrode[29], was calculated from the diameter in the real-part impedance of high-frequency distorted semi-circle (shown in Fig.5b). It is obvious that the R_{ct} of non-DR-GO/PPy is always smaller than that of DR-GO/PPy at each application potential, indicating that the ion insertion into the outer layer of dense DR-GO/PPy composite and the electron transfer along solid phase matrix has been hindered to a certain extent. Moreover, based on the transmission line model[23, 31], the significant increase in the system resistance at the low-frequency region for DR-GO/PPy electrode demonstrate that it has larger anomalous ion diffusion resistance in the micropore and the charge-transfer resistance at the distribution interface (parallel to outer interface) of the composite matrix.

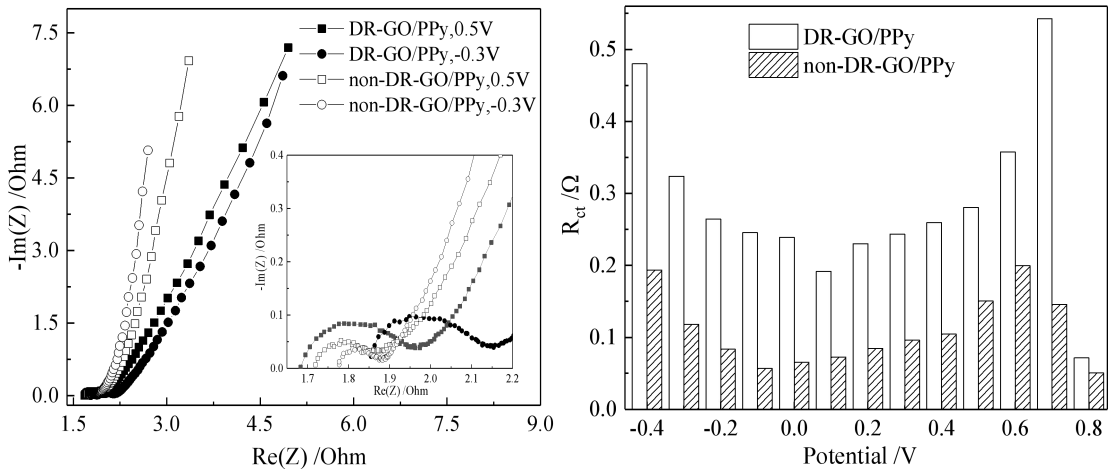

Fig. 5. The Nyquist spectra of two GO/PPy electrode at different d.c. potential (a), and the calculated charge transfer resistance, R_{ct}, from the high-frequency impedance spectra (b).

The specific capacitance of the two GO/PPy composite electrodes as a function of the frequency at different potentials are calculated from the impedance spectra according to the equation (1) and shown in Fig.6a. As the frequency decreases, the potential perturbation gradually reach the micropore distributing deeply inside the composite, thus the capacitivity of two composite electrode all increase rapidly[32]. Comparatively, at different application potential, the DR-GO/PPy composite still displays smaller low-frequency capacitance than that of non-DR-GO/PPy, indicating the less charging density on polymeric backbone of DR-GO/PPy. Fig. 6b shows the normalized EIS differential capacity curves for two electrodes at the frequency of 0.01Hz. It can be observed that the PZC of non-DR-GO/PPy is about 0.5V, which is more positive than the PZC of PPy doped with Cl^- and nearly close to that of PPy doped with bulky anions[19]. It may be relevant to the plenty of carboxyl group with negative charge on the surface and edge of GO nanosheets (as shown in Fig.4S). In the case of DR-GO/PPy, the PZC is positive shifted to about 0.7V, that is to say, an higher oxidation overpotential is needed to produce enough polaron and bipolaron for neutralizing the similar charging density of GO component as that in non-DR-GO/PPy composite. In conclusion, from the variation of ohmic resistance and redox capacitance responses between the two composite, it is reasonable to consider that the densely entanglement polymeric chain and the strong interactions arising from deep reduction, have greatly hindered the conformational transformation of PPy during the redox, which inclines to induce less doping level and more stabilizing polaronic structure of polymeric backbone. The conformational and electronic state structure characteristic not only is detrimental to the solid-phase electron transformation, but also will influence the ions intercalation/desintercalation in the electro-sorption-desorption cyclic process [33].

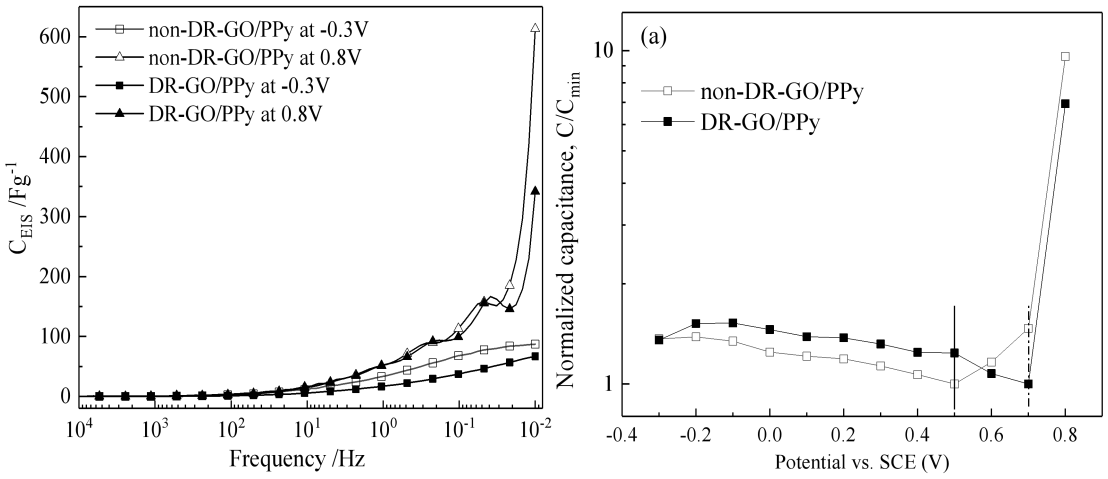

Fig.6. The EIS differential capacity of non-DR-GO/PPy and DR-GO/PPy composite electrodes at different d.c. potential as a function of frequency (a), and the normalized EIS differential capacity (at the frequency of 0.01Hz) curves of two electrodes as a function of application potential (b).

3.4 MCDI desalination performance

Comparison of the desalination performance of non-DR-GO/PPy and DR-GO/PPy electrode were implemented in a MCDI cell by varying the concentration of NaCl solution from 200mg/L to 1000mg/L. The use of a MCDI configuration is particularly essential to assemble test cell by a pair of the same faradic electrodes. Fig.5S(a-c) displays the stable conductivity and current curves of non-DR-GO/PPy and DR-GO/PPy after the first five cycles. Obviously, at the beginning of electro-sorption stage, the conductivity of the effluent solution passing through the MCDI cell decreases quickly after 1.2 V of d.c. potential applied. As time goes on, the conductivity drops slowly until reaching the electro-sorption equilibrium (the electro-sorption is nearly saturated), and then gradually returns to the initial high value due to the continuous supply of feed water. As shown in the Fig.5S(a), the DR-GO/PPy electrode leads to a decrease in the conductivity from 420 to 380 μS/cm, while it decreases from 420 to 336 μS/cm when of utilizing the non-DR-GO/PPy electrode, which indicates a 210% increase in the desalination efficiency. When the

salinity of feed water increases to 500mg/L and 1000mg/L, the desalination efficiency shown in Fig.5S(b) and Fig.5S(c) has increased to 317% and 259%, respectively. It confirms that the polymeric conformatioal variation has greatly influence the electro-sorption performance of GO/PPy composite electrode.

Fig. 7a and 7b represents the salt adsorption capacity normalized to the active mass (SAC) of the two electrodes as a function of time for electro-sorption experiments using different NaCl concentrations. A pseudo-first-order model (Eq. (2)) was employed to determine the equilibrium ion adsorption capacity and the rate constant through linear regression [17].

$$\ln \frac{q_e}{q_e - q_t} = kt \qquad (2)$$

where q_e and q_t are the salt adsorption capacity normalized to the active mass of the electrode (mg/g) at equilibrium state and at time t (s), respectively, k is pseudo-first-order rate constant (s^{-1}).

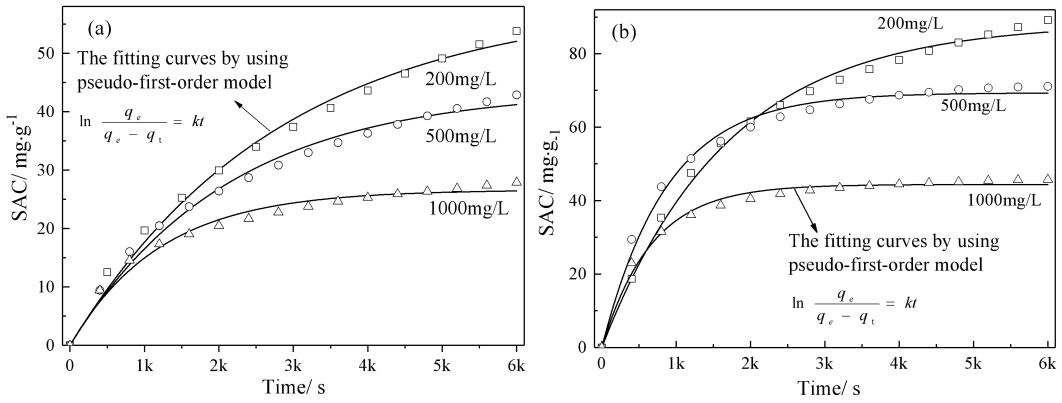

Fig.7. Fitting electrosorption curves of DR-GO/PPy (a) and non-DR-GO/PPy electrode (b) with a pseudo-first-order kinetics model. The dots represent q_t calculated from the experimental data (shown in Fig.S4) and the solid lines are the regression lines.

The regression coefficients and R^2 values (coefficient of determination) were listed in Tab.2. It is clearly shown that the pseudo-first-order model approximates the experimental data well for two test material in every influent concentration. The non-DR-GO/PPy electrode, as expected, exhibits a larger ion electrosorption capacity

and rate constant than the other electrode. These results are well corresponding to the previous analysis of XPS and EIS. The difference of overall electro-sorption performance is believed to be directly linked to the structural factors of conducting polymer component in composite. The less electro-sorption sites on polymer chain and more densely packing polymeric structure generally can decrease ion migration and storage into the composite matrix, thus display as a suppression electrosorption dynamic process.

Table.2. Model fitting results for MCDIs with two electrode materials.

electrode	DR-GO/PPy			non-DR-GO/PPy		
Influent concentration （mg/L）	200	500	1000	200	500	1000
q_e(mg/g)	59.06	43.74	26.60	88.43	69.35	44.38
k(s^{-1})	0.000355	0.000474	0.000812	0.000592	0.00115	0.00151
R^2	0.9927	0.9906	0.9810	0.9954	0.9910	0.9888

In addition, when the influent concentration of MCDI cell increase from 200mg/L to 1000mg/L, the saturated electro-sorption capacity decline obviously for both two composite electrodes, and it is fairly different with the behavior of MCDI cell assembled by conventional carbon electrode in the condition of various influent concentration [34~36]. The reason for these difference is proposed to be closely related to the installed cation and anion exchange membrane (named as CEM and AEM, respectively) in the symmetrical test cell and typical electro-sorption mechanism of conducting polymer. Based on the well-studied electrochemical redox process of PPy, the reduced composite electrode is oxidized at a positive potential to produce polaron and bipolaron on polymer backbone, and is accompanied by the polymer structure opening and conformational relaxing. To neutralize the residual charges of the positive electrode, counter-ions (Cl^-) in the bulk solution simultaneous penetrate the AEM in front of the electrode and move into the composite matrix by diffusion

control (as shown in scheme.1). Meanwhile, the oxidized polymer in the negative electrode experiences the opposite process. Due to the blocking effect of CEM in front of the negative electrode, the released chloride ions from composite can not permeate through the membrane, then sodium ions from the bulky solution spontaneous penetrate the CEM to achieve charge balance. Thus, at the subsequent electro-desorption process, it is more difficult to complete release "co-ions" from the gap between CEM and negative electrode, in which the cations and anions have all involved in the redox process of PPy component due to the co-ion effect as reported before[37, 38]. In this sense, the measured saturated capacity listed in Tab.2 should be less than its real electro-sorption extreme. If the concentration of feed water increases, the amount of ions accumulation at the gap will increase proportionally, inducing the co-ions effect more significant and then the desalination process less efficient. Thus, an inverse relationship between saturated electro-sorption capacity and the concentration of feed water is observed. In the light of these cases, assemble capacitive deionization cell with asymmetrical composite electrode (asymmetry exist between the zero-charge potential of cathode and anode) is thought to be an alternative implementations for exerting the merit of faradic composite electrode material in capacitive deionization process.

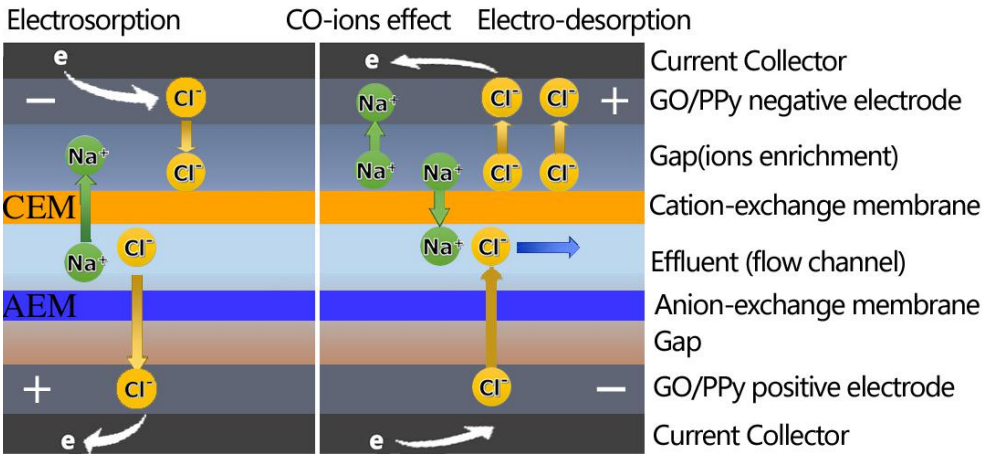

Scheme.1 Schematic diagram about the role of ion-exchange membrane in MCDI assembled with GO/PPy composite electrode

4. Conclusion

In this study, a cyclic voltammetric treatment method with different low limit of potential window were used to manipulate the degree of polymeric conformational shrink, which can not complete relaxed or opened after subsequent oxidation process. This structural irreversible change of GO/PPy composite was confirmed by SEM, FTIR, XPS and EIS techniques, which makes it possible to analyze the influence of polymeric conformational change on the electrosorption performance of faradic GO/PPy composite electrode without the interference of dopant. When the low limit of potential window is shifted to a potential negative enough, the densely packing structure of obtained DR-GO/PPy induces the strengthening intermolecular force between neighboring polymer chain and a morphological change in the composite matrix. Both results in the loss of charging density or π-electron delocalization degree on polymer backbone due to the less doping level. Therefore, the electrochemical performance is damaged with the main characteristic of increase in the charge transfer resistance (R_{ct}) of the composite/solution interface, and decrease in EIS differential capacity (C_{EIS}). Then, the saturated electro-sorption capacity of GO/PPy composite electrode decreases obviously.

Moreover, in the case of carbon-based conducting polymer electrode, the ion-exchange membrane can not eliminate the co-ions effect of MCDI cell assembled by the symmetrical faradic composite electrode due to the typical electrosorption mechanism of conducting polymer. The ions accumulation in the gap between CEM and negative electrode makes it possible for cations and anions to participate the redox process of PPy without membrane blocking. Therefore, the saturated electro-sorption capacity of GO/PPy electrode has an unusual inverse relationship with the increase concentration of feed water. Consider from this aspect, it can be speculated that the capacitive deionization cell with asymmetrical faradic electrode (asymmetry exist between the zero-charge potential of cathode and anode) has the

merit of improving the salt removal efficiency in the high salinity solution.

Acknowledgements

This subject is supported by China Ministry of Science and Technology as “the National Key Research and Development Plan (Project No. SQ2018YFE010367)” and the Special Fund for Basic Scientific Research Business of Central Public Research Institutes (Project No. K-JBYWF-2019-T07 and K-JBYWF-2016-T03).

References

[1] M. Elimelech, W.A. Phillip. The future of seawater desalination: energy, technology, and the environment. Science, 2011, 333: 712-717.

[2] M.A. Shannon, P.W. Bohn, M. Elimelech, J.G. Georgiadis, B.J. Mariñas, A.M. Mayes. Science and technology for water purification in the coming decades, Nature, 2008, 452: 301-310.

[3] A. Drak, M. Adato. Energy recovery consideration in brackish water desalination. Desalination, 2014, 339: 34-39.

[4] M.A. Anderson, A.L. Cudero, J. Palma. Capacitive deionization as an electrochemical means of saving energy and delivering clean water. Comparison to present desalination practices: will it compete? Electrochim. Acta, 2010, 55: 3845-3856.

[5] A.A. Faisal, A.A. Amal, S. Irfan , H. Nidal. Application of Capacitive Deionisation in water desalination: A review. Desalination, 2014, 342: 3-15.

[6] A. Subramani, J.G. Jacangelo, Emerging desalination technologies for water treatment: A critical review. Water Res., 2015, 75: 164-187.

[7] M.A. Ahmed, S. Tewari, Capacitive deionization: Processes, materials and state of the technology. J. Electroanal. Chem., 2018, 813:178-192.

[8] S.I. Wong, J. Sunarso, B.T. Wong, H. Lin, A. Yu, B. Jia, Towards enhanced energy density of graphene-based supercapacitors: Current status, approaches, and future directions. J. Power Sources, 2018, 396: 182–206.

[9] J. Zhang, J. Wang, J. Yang, Y. Wang, M. B. Chan-Park, Three-dimensional macroporous graphene foam filled with mesoporous polyaniline network for high areal capacitance. ACS Sustainable Chem. Eng., 2014, 2: 2291-2296.

[10] G. Xin, Y. Wang, X. Liu, J. Zhang, Y. Wang, J. Huang, J. Zang, Preparation of self-supporting graphene on flexible graphite sheet and electrodeposition of polyaniline for supercapacitor. Electrochim. Acta, 2015, 167: 254-261.

[11] P. Sekar, B. Anothumakkool, S. Kurungot, 3D Polyaniline Porous Layer Anchored Pillared Graphene Sheets: Enhanced Interface Joined with High Conductivity for Better Charge Storage Applications. ACS Appl. Mater. Interf., 2015, 7: 7661-7669.

[12] C. Yang, L. Zhang, N. Hu, Z. Yang, H. Wei, Z. Xu, Y. Wang, Y. Zhang, Densely-packed graphene/conducting polymer nanoparticle papers for high-volumetric-performance flexible all-solid-state supercapacitors. Appl. Surf. Sci, 2016, 379: 206-212.

[13] Y. Liu, K. Xu, X. Zhang, C. Qi, Q. Lv, H. Feng, Electrochemical codeposition of graphene/polypyrrole composites on carbon paper for electrochemical capacitors. Curr. Appl. Phys., 2016, 16(5): 520-526.

[14] J.J. Fang, K. Xu, L.H. Zhu, Z.X. Zhou, H.Q. Tang. A study on mechanism of corrosion protection of polyaniline coating and its failure. Corros. Sci., 2007, 49: 4232-4242.

[15] Kavita Pandey, Pankaj Yadav and Indrajit Mukhopadhyay. Elucidating the effect of copper as a redox additive and dopant on the performance of a PANI based supercapacitor. Phys. Chem. Chem. Phys., 2015, 17(2): 878-887.

[16] S. Leguizamon, K.P. Díaz-Orellana, J. Velez, M.C. Thies, M.E. Roberts. High charge-capacity polymer electrodes comprising alkali lignin from the Kraft process. J. Mater. Chem. A, 2015, 3: 11330-11339.

[17] Y. Cai, Y. Wang, X. Han, L. Zhang, S. Xu, J. Wang, Optimization on electrode assemblies based on ion-doped polypyrrole/ carbon nanotube composite in capacitive deionization process. J. Electroanal. Chem., 2016, 768: 72-80.

[18] C. Yan, L. Zou, R. Short, Polyaniline-modified activated carbon electrodes for capacitive deionization. Desalination, 2014, 333: 101-106.

[19] D. Ma, Y. Wang, X. Han, S. Xu, J. Wang, Applicable tolerance evaluations of ion-doped carbon nanotube/polypyrrole electrode under adverse solution conditions for capacitive deionization process. Sep. Purif. Technol., 2018, 201: 167-178.

[20] K. Xu, L.H. Zhu, A.Q. Zhang, G.D. Jiang, H.Q. Tang. A peculiar cyclic voltammetric behavior of polyaniline in acetonitrile and its application in ammonia vapor sensor. J. Electroanal. Chem., 2007, 608: 141-147.

[21] A. Omosebi, X. Gao, J. Rentschler, J. Landon, K. Liu. Continuous operation of membrane capacitive deionization cells assembled with dissimilar potential of zero charge electrode pairs. J. Colloid. Interf. Sci., 2015, 446: 345-351.

[22] L. Chang, W. Wei, K. Sun, Y.H. Hu. 3D flower-structured graphene from CO_2 for supercapacitors with ultrahigh areal capacitance at high current density. J. Mater. Chem. A, 2015, 3: 10183-10187.

[23] L.F.Q.P. Marchesi, F.R. Simóes, L.A. Pocrifka, E.C. Pereira. Investigation of Polypyrrole Degradation Using Electrochemical Impedance Spectroscopy. J. Phys. Chem. B, 2011, 115: 9570-9575.

[24] T. Raudsepp, M. Marandi, T. Tamm, V. Sammelselg, J. Tamm. Study of the factors

determining the mobility of ions in the polypyrrole films doped with aromatic sulfonate anions. Electrochim. Acta, 2008, 53: 3828-3835.

[25] Y. Liu, H. Wang, J. Zhou, L.Y. Bian, E.W. Zhu, J.F. Hai, J. Tang, W.H. Tang. Graphene/polypyrrole intercalating nanocomposites as supercapacitors electrode. Electrochim Acta, 2013, 112: 44-52.

[26] D.C. Zhang, X. Zhang, Y. Chen, P. Yu, C.H. Wang, Y.W. Ma. Enhanced capacitance and rate capability of graphene/polypyrrole composite as electrode material for supercapacitors. J. Power Sources, 2011, 196: 5990-5996.

[27] C.Z. Zhu, J.F. Zhai, D. Wen, S.J. Dong. Graphene oxide/polypyrrole nanocomposites: one-step electrochemical doping, coating and synergistic effect for energy storage. J. Mater. Chem., 2012, 22, 6300-6306.

[28] A. Österholm, T. Lindfors, J. Kauppila, P. Damlin, C. Kvarnström. Electrochemical incorporation of graphene oxide into conducting polymer films. Electrochim. Acta, 2012, 83: 463-470.

[29] Y. Song, J.L. Xu, X.X. Liu. Electrochemical anchoring of dual doping polypyrrole on graphene sheets partially exfoliated from graphite foil for high-performance supercapacitor electrode. J. Power Sources, 2014, 249: 48-58.

[30] R. Bouldin, S. Ravichandran, A. Kokil, R. Garhwal, S. Nagarajan, J. Kumar, F.F. Bruno, L.A. Samuelson, R. Nagarajan. Synthesis of polypyrrole with fewer structural defects using enzyme catalysis. Synth. Met., 2011, 161: 1611-1617.

[31] G.G. Belmonte, J. Bisquert, E.C. Pereira, F.F. Santiago. Switching behaviour in lightly doped polymeric porous film electrodes. Improving distributed impedance models for mixed conduction conditions. J. Electroanal. Chem. 2001, 508, 48-58.

[32] R.L. Zornitta, F.J. García-Mateos, J.J. Lado, J. Rodríguez-Mirasol, T. Cordero, P. Hammer, L.A.M. Ruotolo. High-performance activated carbon from polyaniline for capacitive deionization. Carbon, 2017, 123: 318-333.

[33] S. Mondal, M.V. Sangaranarayanan. Permselectivity and thickness-dependent ion transport properties of overoxidized polyaniline: a mechanistic investigation. Phys. Chem. Chem. Phys., 2016, 18(44): 30705-30720.

[34] Y.J. Zhao, Y. Wang, R.G. Wang, Y.F. Wu, S.C. Xu, J.X. Wang. Performance comparison and energy consumption analysis of capacitive deionization and membrane capacitive deionization processes. Desalination, 2013, 324: 127-133.

[35] C.J. Feng, Y.A. Chen, C.P. Yu, C.H. Hou. Highly porous activated carbon with multi-channeled structure derived from loofa sponge as a capacitive electrode material for the deionization of brackish water. Chemosphere, 2018, 208: 285-293.

[36] Z.Y. Leong, G. Lu, H.Y. Yang. Three-dimensional graphene oxide and polyvinyl alcohol composites as structured activated carbons for capacitive desalination. Desalination, 2019, 451: 172-181.

[37] A. Hassanvand, G.Q. Chen, P.A. Webley, S.E. Kentish. A comparison of multicomponent electrosorption in capacitive deionization and membrane capacitive deionization. Water Res., 2018, 131: 100-109.

[38] J. Yu, K. Jo, T. Kim, J. Lee, J. Yoon. Temporal and spatial distribution of pH in flow-mode capacitive deionization and membrane capacitive deionization. Desalination, 2018, 439: 188-195.